Finite element analysis of the initiation of landslides with a multiphase model

L. Sanavia & B.A. Schrefler
Department of Structural and Transportation Engineering, University of Padua, Padua, Italy

ABSTRACT: Finite element analysis of the initiation of landslides due to capillary and water pressure variation is presented. To this aim, a non-isothermal elasto-plastic multiphase material model for soils is used. Soils are modeled as a three-phase deforming porous continuum where heat, water and gas flow are taken into account. In particular, the gas phase is modeled as an ideal gas composed of dry air and water vapor. Phase changes of water (evaporation-condensation, adsorption-desorption), heat transfer through conduction and convection and latent heat transfer are considered. The macroscopic balance equations are discretized in space and time within the finite element method. The independent variables are the solid displacements, the capillary and the gas pressure and the temperature. The effective stress state is limited by Drucker-Prager yield surface for simplicity. Small strains and quasi-static loading conditions are assumed. Numerical results of a slope stability experiment are presented assuming plane strain condition during the computations.

1 MATHEMATICAL MODEL

The full mathematical model necessary to simulate the thermo-hydro-mechanical transient behavior of fully and partially saturated porous media is developed in Lewis & Schrefler (1998) using averaging theories. The underlying physical model is briefly summarized in the present section for sake of completeness.

The partially saturated porous medium is treated as multiphase system composed of $\pi = 1,\ldots,$ k constituents with the voids of the solid skeleton (s) filled with water (w) and gas (g). The latter is assumed to behave as an ideal mixture of two species: dry air (noncondensable gas, ga) and water vapor (condensable one, gw). Using spatial averaging operators defined over a representative elementary volume R.E.V., the microscopic equations are integrated over the R.E.V. giving the macroscopic balance equations (Lewis & Schrefler 1998).

At the macroscopic level the porous media material is modeled by a substitute continuum that fills the entire domain simultaneously, instead of the real fluids and the solid which fill only a part of it. In this substitute continuum each constituent p has a reduced density which is obtained through the volume fraction. In the general model developed in Lewis & Schrefler (1998) inertial forces, heat conduction, vapor diffusion, heat convection, water flow due to pressure gradients or capillary effects and latent heat transfer due to water phase change (evaporation and condensation) inside the pores are taken into account. The solid is deformable and non-polar, and the fluids, the solid and the thermal fields are coupled. All fluids are in contact with the solid phase. The constituents are assumed to be isotropic, homogeneous, immiscible except for dry air and vapor, and chemically non reacting. Local thermal equilibrium between solid matrix, gas and liquid phases is assumed, so that the temperature is the same for all the constituents. The state of the medium is described by capillary pressure p^c, gas pressure p^g, temperature T and displacements of the solid matrix $\boldsymbol{u}$ (see e.g. Sanavia et al. 2005b for a discussion concerning the choice of the independent variables). In the partially saturated zones water is separated from its vapor by a concave meniscus (capillary water). Due to the curvature of this meniscus the sorption equilibrium equation (e.g. Lewis & Schrefler 1998) gives the relationship between the capillary pressure p^c and the gas p^g and water pressure p^w

$$p^c = p^g - p^w \tag{1}$$

Pore pressure is defined as compressive positive for the fluids, while stress is defined as tension positive for the solid phase.

Moreover, in multiphase materials theory it is common to assume the motion of the solid as a reference and to describe the fluids in terms of motion relative to the solid. This means that a fluid relative velocity with respect to the solid is introduced. The fluid relative velocity $\boldsymbol{v}^{\pi s}$ or diffusion velocity is

given by $\boldsymbol{v}^{\pi s} = \boldsymbol{v}^{\pi} - \boldsymbol{v}^{s}$, with $\pi = g, w$, and will be described by the Darcy law.

The macroscopic balance equations of the implemented model are now summarized. These equations are obtained introducing the following assumptions in the model developed in Lewis & Schrefler (1998):

- at the micro level, the porous medium is assumed to be constituted of incompressible solid and water constituents, while gas is considered compressible;
- the process is considered as quasi-static.

The interested reader can refer to Sanavia et al. (2005a,b) for the development of this model.

1.1 *Linear momentum balance equations*

The linear momentum balance equation of the mixture in terms of total Cauchy stress $\boldsymbol{\sigma}$ assumes the form

$$div\boldsymbol{\sigma} + \rho\boldsymbol{g} = \boldsymbol{0} \tag{2}$$

where ρ is the density of the mixture

$$\rho = [1-n]\rho^{s} + nS_{w}\rho^{w} + nS_{g}\rho^{g} \tag{3}$$

with n the porosity, ρ^{π} the density of the π-phase and S_w and S_g the water and gas degree of saturation, respectively. The total Cauchy stress can be decomposed into the effective and pressure (equilibrium) parts following the principle of effective stress

$$\boldsymbol{\sigma} = \boldsymbol{\sigma}' - \left[S_{g}\, p^{g} + S_{w} p^{w}\right]\mathbf{1} \tag{4}$$

where $\boldsymbol{\sigma}'$ is the modified effective Cauchy stress tensor (also called Bishop's stress tensor in soil mechanics) and $\mathbf{1}$ is the second order identity tensor.

1.2 *Mass balance equations*

The mass conservation equation for the solid skeleton, the water and the vapor is

$$\begin{aligned}
&n\left[\rho^{w} - \rho^{gw}\right]\frac{\partial S_{w}}{\partial t} + \left[\rho^{w} S_{w} - \rho^{gw}[1-S_{w}]\right] div\left(\frac{\partial \boldsymbol{u}}{\partial t}\right) \\
&+ [1-S_{w}] n \frac{\partial \rho^{gw}}{\partial t} - div\left(\rho^{w}\frac{\boldsymbol{k}k^{rw}}{\mu^{w}}\left[grad\left(p^{w}\right) - \rho\boldsymbol{g}\right]\right) \\
&- div\left(\rho^{g}\frac{M_{a}M_{w}}{M_{g}^{2}}\boldsymbol{D}_{g}^{gw} grad\left(\frac{\partial p^{gw}}{\partial p^{c}}\right)\right) \\
&- div\left(\rho^{gw}\frac{\boldsymbol{k}k^{rg}}{\mu^{g}}\left[grad\left(p^{g}\right) - \rho\boldsymbol{g}\right]\right) - \beta_{swg}\frac{\partial T}{\partial t} = 0
\end{aligned} \tag{5}$$

where $\boldsymbol{k}$ is the intrinsic permeability tensor, k^{rw} the water relative permeability and μ^{w} the water viscosity. Similarly for k^{rg} and μ^{g}. β_{swg} combines the solid, liquid and gas cubic thermal expansion coefficients (Lewis & Schrefler 1998). The inflow and outflow fluxes have been described using the Fick law for the diffusion of the vapor in the gas phase and using the Darcy law for the water and the gas flows.

Similarly, the mass balance equation for the dry air is

$$\begin{aligned}
&\rho^{ga}\left[n\frac{\partial S_{w}}{\partial t} + S_{g}\, div\left(\frac{\partial \boldsymbol{u}}{\partial t}\right)\right] + nS_{g}\left[\frac{\partial \rho^{ga}}{\partial t} + \frac{\partial \rho^{ga}}{\partial p^{g}}\right] \\
&- div\left(\rho^{g}\frac{M_{a}M_{w}}{M_{g}^{2}}\boldsymbol{D}_{g}^{ga} grad\left(\frac{p^{ga}}{p^{g}}\right)\right) \\
&- div\left(\rho^{ga}\frac{\boldsymbol{k}k^{rg}}{\mu^{g}}\left[grad\left(p^{g}\right) - \rho^{g}\boldsymbol{g}\right]\right) \\
&- \beta_{s}\rho^{ga}[1-n]S_{g}\frac{\partial T}{\partial t} = 0
\end{aligned} \tag{6}$$

The quantities S_w, S_g, k^{rw} and k^{rg} are defined at the constitutive level, as described in a following Section.

1.3 *Energy balance equation*

The energy balance equation of the mixture is

$$\begin{aligned}
&\left(\rho C_{p}\right)_{eff}\frac{\partial T}{\partial t} - div\left(\chi_{eff}\; grad(T)\right) \\
&+ \rho^{w} C_{p}^{w}\left[\frac{\boldsymbol{k}k^{rw}}{\mu^{w}}\left[-\,grad\left(p^{w}\right) + \rho^{w}\boldsymbol{g}\right]\right] grad(T) \\
&- \rho^{g} C_{p}^{g}\left[\frac{\boldsymbol{k}k^{rg}}{\mu^{g}}\left[grad\left(p^{g}\right) - \rho^{g}\boldsymbol{g}\right]\right] grad(T) \\
&- \beta_{s}\rho^{ga}[1-n][1-S_{w}]\frac{\partial T}{\partial t} = -\dot{m}_{vap}\Delta H_{vap}
\end{aligned} \tag{7}$$

where, in particular, $\dot{m}_{vap}\Delta H_{vap}$ takes into account the contribution of the evaporation and condensation.

Initial and boundary conditions (Lewis & Schrefler 1998, Sanavia et al. 2005a,b) together with the constitutive equations close the model.

2 CONSTITUTIVE EQUATIONS

The pressure p^{g} is described in the sequel. For a gaseous mixture of dry air and water vapour, the ideal gas law is introduced because the moist air is assumed to be a perfect mixture of two ideal gases. The equation of state of perfect gas (the Clapeyron equation) and Dalton's law applied to dry air (ga), water vapour (gw) and moist air (g), yield

$$p^{ga} = \rho^{ga} RT / M_{a} \qquad p^{gw} = \rho^{gw} RT / M_{w} \tag{8}$$

$$p^g = p^{ga} + p^{gw} \qquad \rho^g = \rho^{ga} + \rho^{gw} \tag{9}$$

where, in the partially saturated zones, the equilibrium water vapour pressure p^{gw} can be obtained from the Kelvin-Laplace equation (e.g. Lewis & Schrefler 1998).

The saturation S_π and the relative permeability $k^{r\pi}$ are experimentally determined function of the capillary pressure p^c and the temperature T.

For the binary gas mixture of dry air and water vapor, Fick's law gives the relative velocities of the diffusing species.

The elasto-plastic behaviour of the solid skeleton is described within the classical elasto-plasticity theory for geometrically linear problems. The yield function restricting the effective stress state $\boldsymbol{\sigma}'$ is developed in the form of Drucker-Prager for simplicity. The return mapping and the consistent tangent operator are developed, solving the singular behaviour of the Drucker-Prager yield surface in the zone of the apex using the concept of multi-surface plasticity. The return mapping algorithm and the consistent tangent moduli used for the numerical simulations are derived in Sanavia et al. (2005b) for isotropic linear hardening/softening and volumetric-deviatoric non-associative plasticity.

3 FINITE ELEMENT FORMULATION

The finite element model is derived by applying the Galerkin procedure to the spatial integration and the Generalised Trapezoidal Method to the time integration of the weak form of the balance equations introduced in a previous Section (e.g. Lewis & Schrefler 1998).

In particular, after spatial discretisation within the isoparametric formulation, a non-symmetric, non-linear and coupled system of equation is obtained.

After time integration, the non-linear system of equation is linearized, thus obtaining the equations system that can be solved numerically. Details concerning the matrices and the residuum vectors of the linearized equations system can be found in Sanavia et al. (2005b). Owing to the strong coupling between the mechanical and the pore fluid problem, a monolithic solution is preferred using a Newton scheme.

4 EXPERIMENTAL RESULTS

A 2-D laboratory test was carried out by G. Klubertanz during his PhD thesis at LMS-EPFL in Lausanne (Klubertanz 1999, Klubertanz et al. 2003). The experiment reproduces a stability problem of a slope of 1 m hight and 1.5 m in length (Fig. 1). A constant water table was imposed at the left- and right-hand sides of the slope below the upper surface (at 0.2 and 0.15 m, respectively) and the material was initially partially saturated. During the experiment, the authors applied a constant water pressure of 1.6 kPa at the left part of the bottom surface. The authors observed the first failure of the lower part of the slope after about 80 s since the application of the water load. The slope continued to fail by backward erosion and outflow appeared at the lower part afterwards. During the experiment, the authors measured water and gas pressure and solid displacements.

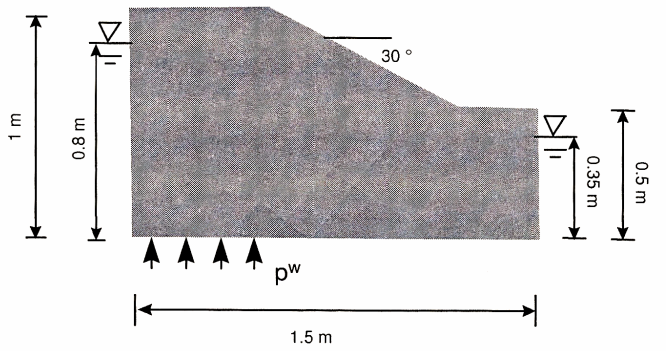

Figure 1. Description of the geometry of the experimental test and of the boundary and loading conditions (Klubertanz 1999).

5 NUMERICAL RESULTS

A finite element analysis of the Klubertanz experimental test has been performed with the multiphase model presented in the previous sections. Some of the material parameters have been chosen from the laboratory test; the value of cohesion was selected in order to get the failure of the slope at about 90 s with a dilatancy angle of 0°. The material parameters used in the computation are listed in Table 1.

The solid skeleton is assumed to obey the elasto-plastic Drucker-Prager constitutive model in isothermal condition, with isotropic linear softening behaviour and non-associated plastic flow. The constitutive relationships for the water degree of saturation $S_w(p^c)$ and the water relative permeability $k^{rw}(S_w)$ are of the type of Safai and Pinder in isothermal condition, as plotted in Figure 2 and Figure 3, respectively. For the gas relative permeability $k^{rg}(S_w)$, the relationship of Brooks and Corey in isothermal condition has been selected, as depicted in Figure 3.

Table 1. Material parameters used in the computation.

Solid density	ρ_s	2500	kg/m^3
Water density	ρ_w	1000	kg/m^3
Air density	ρ_g	1	kg/m^3
Young modulus	E	0.43E+06	Pa
Poisson ration	ν	0.46	
Initial apparent cohesion	c_0	420	Pa
Plastic modulus	h	-4.30^E+04	Pa
Friction angle	ϕ	34°	
Dilatancy angle	ψ	0°	
Initial porosity	n	0.415	
Intrinsic permeability	k_w	8.00E-13	m^2

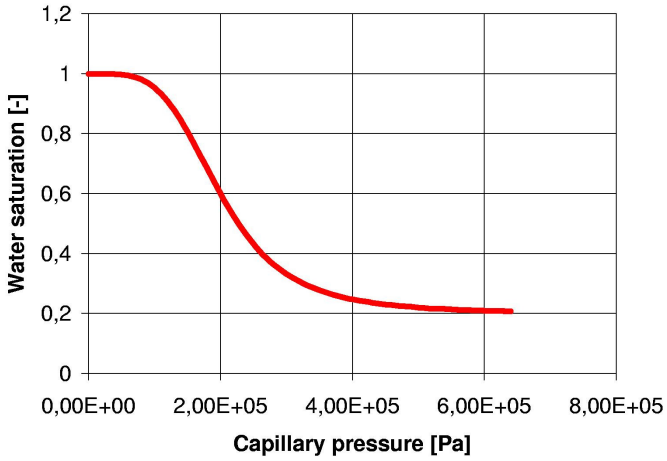

Figure 2. Water degree of saturation S_w function of p^c.

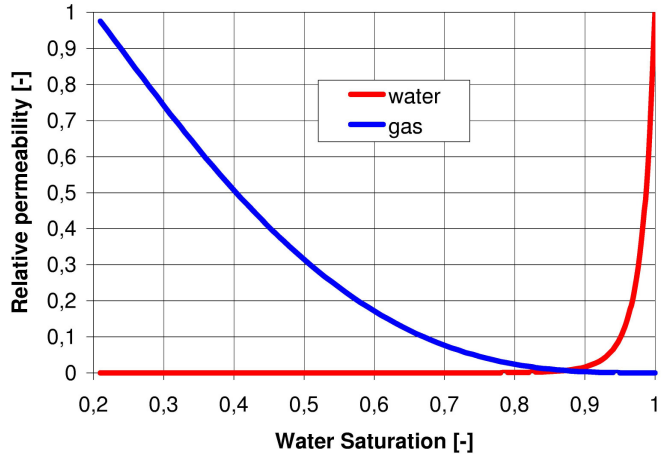

Figure 3. Relative permeability of water and gas.

We have simulated the experimental test applying three runs (the spatial discretisation adopted is depicted in Figure 4).

With the first one, a uniform capillary pressure p^c of 9000 Pa (which correspond to a uniform water saturation S_w of 32%), a uniform ambient temperature and atmospheric pressure were applied to simulate an almost dry material packed within the experimental box. Horizontal displacements of the lateral surfaces and vertical displacements of the lower surface are constrained. The mechanical equilibrium with these thermo-hydro conditions was computed consequently by the model. Then, with the second run, an hydrostatic water load was applied on the lateral surfaces, as depicted in Figure 5. The upper surface is at atmospheric pressure, while the lateral and the lower surfaces are impervious to any fluid flow. The computation was performed until a uniform water flux condition was reached in the domain (see Fig. 6) and the free surface was determined (Fig. 7). The mean pressure p' and the shear stress τ_{xy} are depicted in Figures 8, 9, respectively. It can be observed the lower part of the slope results to be the favourite zone for the initiation of failure because of the lower mean pressure and the higher shear stress. Also the displacements contour reveals that the deformation is higher in the lower part of the slope (Fig. 10).

With the third run, the experimental water load of 1.6 kPa has been applied on the left part of the bottom surface of the slope. The water pressure gradient caused an increase of the level of the free surface up to lower part of the slope, as it can be seen in Figure 11. Failure occurred after 91.5 s, with the plastic strains concentrated in the lower part of the slope (Fig. 12), as experimentally observed in Klubertanz (1999) and described also in klubertanz et al. (2003). At failure, the free surface decreased a little (see Fig. 13) and the maximum water velocity was concentrated in the failure zone (Fig. 14), as experimentally observed.

A closer look inside the plastic zone reveals that the stress state of the material in its natural state (i.e. at the end of the second run) is close to the Drucker-Prager yield surface (Fig. 15) and reach the yield surface because of the increasing of the water pressure (Fig. 16). Once the stress state in on the yield surface, the increasing of water pressure and the softening behaviour of the solid skeleton have the consequences that the stress state remains to the yield surface and hence it continues to develop plastic strains (see Fig. 17) up the failure (at which the cohesion becomes zero because of its softening behaviour).

Temperature and gas pressure at the nodes of the mesh do not change in time and hence their contours have not been included in this paper.

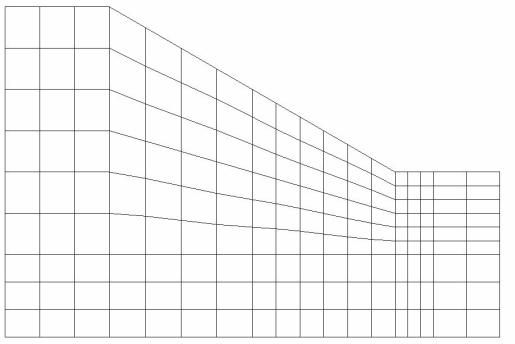

Figure 4. Finite element mesh used for the computations.

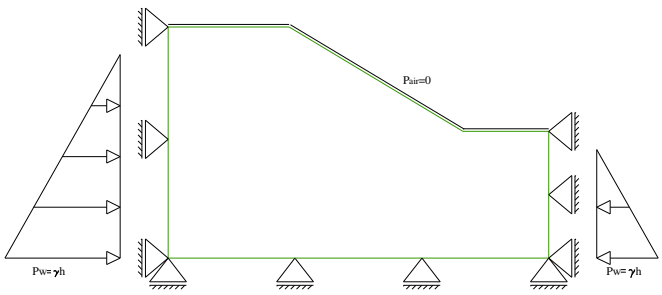

Figure 5. Boundary conditions for the second run.

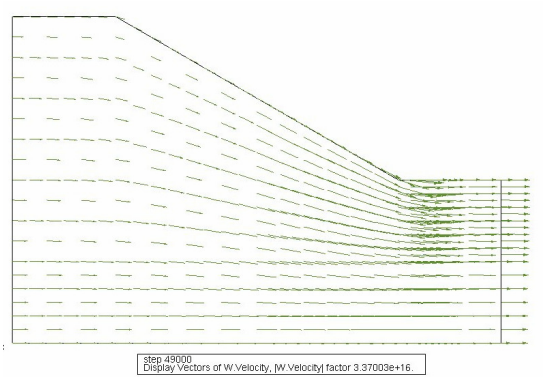

Figure 6. Water flow vectors at the end of the second run.

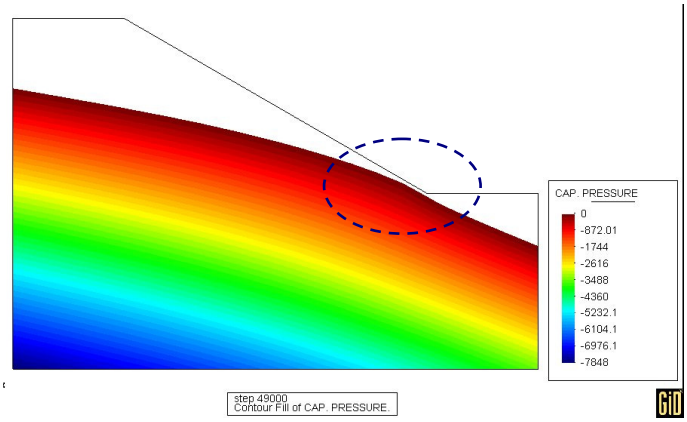

Figure 7. Free surface at the end of the second run.

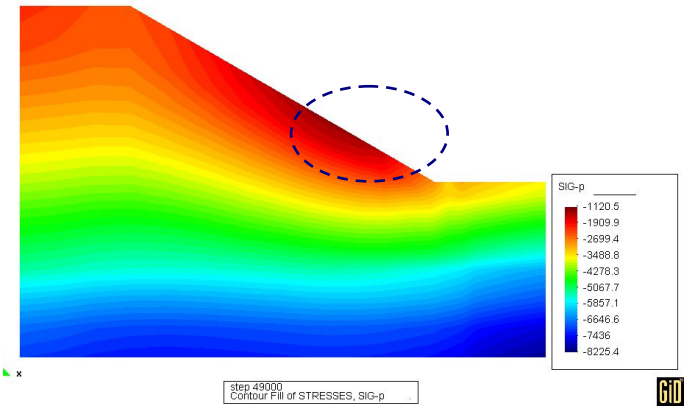

Figure 8. Mean pressure p' at the end of the second run.

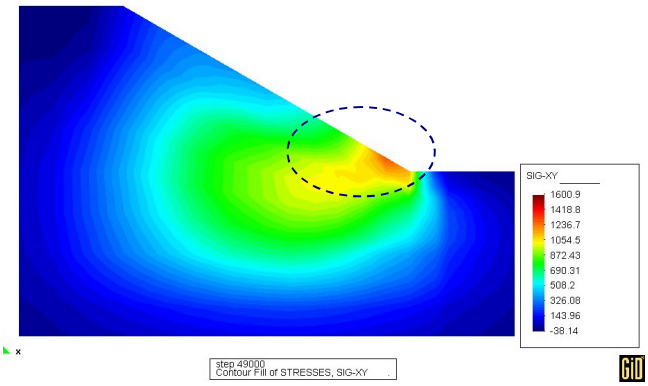

Figure 9. Shear stress τ_{xy} at the end of the second run.

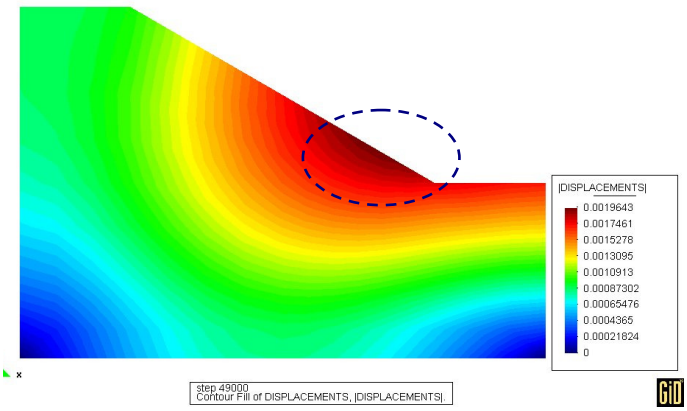

Figure 10. Displacements contour at the end of the second run.

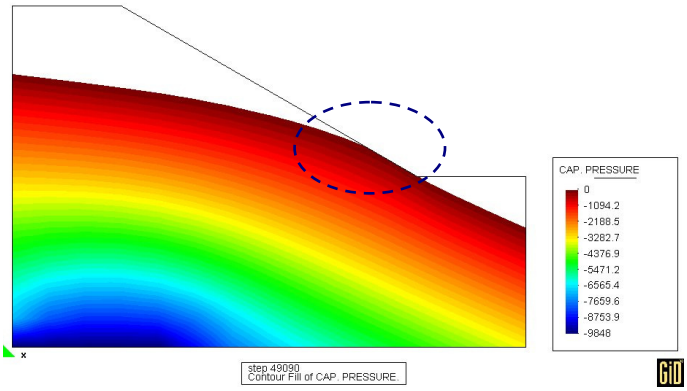

Figure 11. Capillary pressure contour after 90 s of the third run.

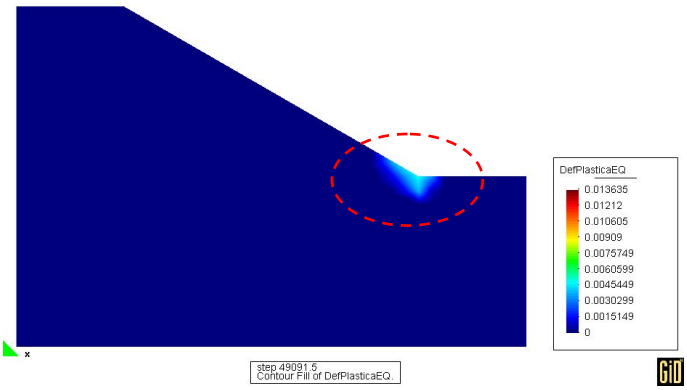

Figure 12. Equivalent plastic strain contour at the end of the third run (91.5 s).

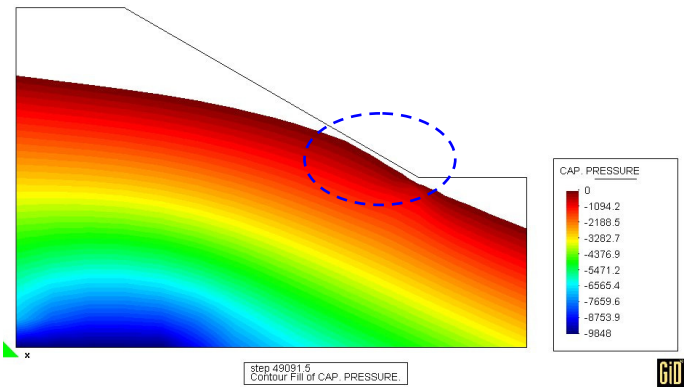

Figure 13. Capillary pressure contour at the end of the third run (91.5 s).

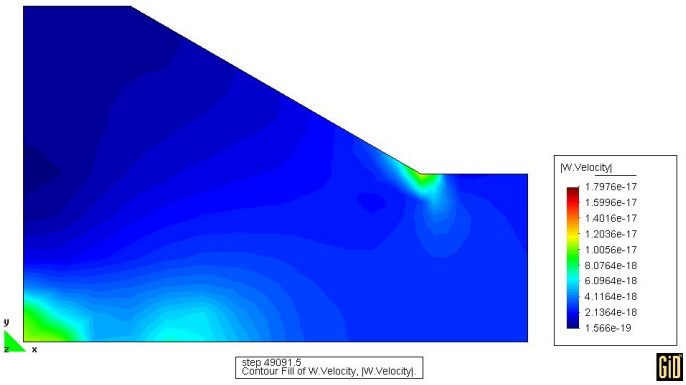

Figure 14. Water velocity contour at the end of the third run (91.5 s).

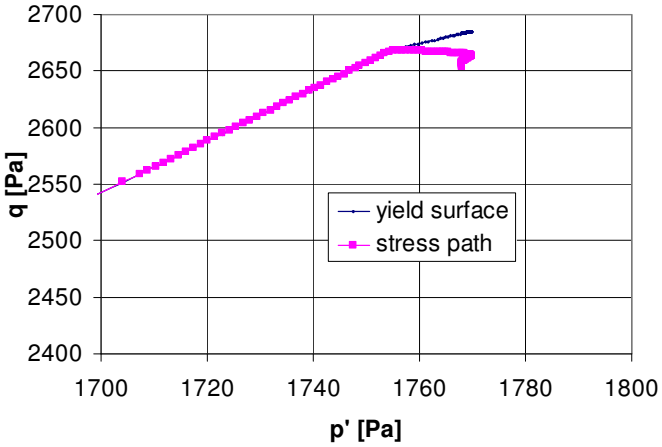

Figure 15. *p'-q* stress path during the third run.

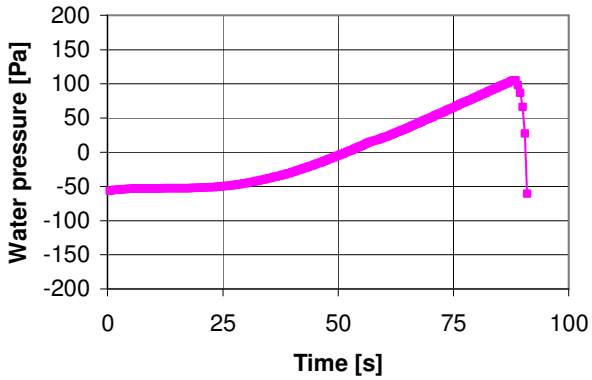

Figure 16. Water pressure vs. time during the third run.

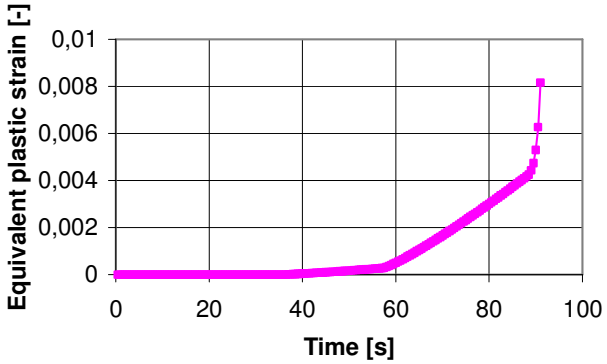

Figure 17. Equivalent plastic strain vs. time during the third run.

6 CONCLUSIONS

A finite element analysis of the initiation of an experimental slope failure has been analyzed in this paper using a non-isothermal elasto-plastic multiphase model. To this end, the formulation for the hydro-thermo-mechanical behaviour of a water saturated and partially saturated porous materials has been presented. This model is obtained as a result of a research in progress on the thermo-hydro-mechanical modelling for multiphase geomaterials undergoing inelastic strains. Then, the numerical results of an experimental test (Klubertanz 1999) have been presented. It has been shown that the first failure zone and outflow appeared at the lower part of the slope have been captured, as experimentally observed.

Acknowledgement

The authors would like to thank the Italian Ministry of Education, University and Research (MIUR 2003081021_004) and the University of Padua (UNIPD CPDA034312) for the financial support.

REFERENCES

Klubertanz G. 1999. *Zur hydromechanischen Kopplung in dreiphasigen porösen Medien*. Thesis n.2027, Lausanne: Ecole Polytechnique Fédérale de Lausanne.

Klubertanz G., Bouchelaghem F., Laloui L., Vulliet L. 2003. Miscible and immiscible multiphase flow in deformable porous media. *Mathematical and Computer Modelling*, 37: 571-582.

Lewis R.W. & Schrefler B.A. 1998. *The Finite Element Method in the Static and Dynamic Deformation and Consolidation of Porous Media.* Chichester: John Wiley & Son.

Sanavia L., Pesavento F., Schrefler B.A. 2005a. Strain localisation simulation in non-isothermal multiphase geomaterials. In T. Schanz (ed.), *Springer Proceedings in Physics; Proc. ISSMGE International Conference From Experimental Evidence towards Numerical Modelling of Unsaturated Soils. Bauhaus University of Weimar, Germany, September 18-19, 2003*. 29-40. Berlin Heidelberg: Springer-Verlag.

Sanavia L., Pesavento F., Schrefler B.A. 2005b. Finite element analysis of non-isothermal multiphase geomaterials with application to strain localisation simulation. *Computational Mechanics* (accepted for publication).